Precambrian Research 278 (2016) 323–336

Contents lists available at ScienceDirect

Precambrian Research

journal homepage: www.elsevier.com/locate/precamres

Discovery of pelitic high-pressure granulite from Manjinggou of the Huai'an Complex, North China Craton: Metamorphic *P–T* evolution and geological implications

Jia-Lin Wu [a], Hua-Feng Zhang [b,*], Ming-Guo Zhai [a,c,*], Jing-Hui Guo [c], Liang Liu [a], Wen-Qiang Yang [a], Hao-Zheng Wang [c], Lei Zhao [c], Xiao-Liang Jia [a], Wei Wang [d]

[a] State Key Laboratory of Continental Dynamics, Department of Geology, Northwest University, Northern Taibai Str. 229, Xi'an 710069, China
[b] School of Earth Sciences and Resources, China University of Geosciences, Xueyuan Road 29#, Haidian District, Beijing 100083, China
[c] Institute of Geology and Geophysics, Chinese Academy of Sciences, Beijing 100029, China
[d] Institute of Geology, Chinese Academy of Geological Sciences, 26 Baiwanzhuang Road, Beijing 100037, China

ARTICLE INFO

Article history:
Received 7 October 2015
Revised 14 February 2016
Accepted 16 March 2016
Available online 24 March 2016

Keywords:
Pelitic and mafic high-pressure granulites
Manjingou
North China Craton
Metamorphic evolution
Paleoproterozoic

ABSTRACT

The first report of Paleoproterozoic mafic high-pressure (HP) granulite terranes in Manjinggou area of the Huai'an Complex, North China Craton (NCC) since 1992 has attracted broad attention from geologists, and accordingly various Early Precambrian continent-continent collision or micro-blocks amalgamation hypotheses were suggested. However, one important issue is still controversial whether the pelitic granulites and associated mafic H*P* granulites underwent similar metamorphic history. Here we report newly recognized pelitic H*P* granulites in Manjinggou area of the Huai'an Complex to provide direct evidence that both pelitic and mafic H*P* granulites suffered similar metamorphic history. The metamorphic peak mineral assemblage of the pelitic granulites is characterized by Grt-Ky-Kfs-Bt-Rt-Qz-Liq±Ms, and the subsequent medium-pressure (M*P*) granulite facies retrogression is characterized by Grt-Sil-Kfs-Pl-Bt-Rt-Liq-Qz. Pseudosection approaches were undertaken in the Na_2O-CaO-K_2O-FeO-MgO-Al_2O_3-SiO_2-H_2O-TiO_2-O (NCKFMASHTO) system to account for textural development, mineral composition and *P–T* evolution of the pelitic granulites. The estimated peak and retrograde granulite facies conditions are 11.5–15 kbar, 810–860 °C and ~9.5 kbar, ~850 °C, respectively, comparable with those of associated mafic H*P* granulites. Consistently, field geological observations and available geochronological data also indicate their similar deformation and metamorphic history from H*P* granulite facies stage (~1.96–1.90 Ga) to retrograde stages (~1.88–1.80 Ga). This finding changes previous views that the pelitic rocks and associated mafic granulites are different slabs with individual metamorphic history. The khondalite series from the Huai'an Complex and adjacent Ji'ning Complex were probably experienced H*P* granulite facies metamorphism, but previously derived M*P* granulite facies conditions might be attributed to mineral re-equilibrium due to long dwell time under M*P* granulite facies. Additionally, these granulite facies rocks record high apparent geothermal gradients and slow exhumation rates relative to H*P*–UH*P* rocks in the Phanerozoic continental collisional orogens. It seems to indicate that the thermal regimes and tectonic mechanisms of Paleoproterozoic probably differ from those of Phanerozoic eons, and these H*T*–H*P* granulite terranes from the NCC were likely formed in a hot and slow cooling orogen.

1. Introduction

Precambrain high-pressure (H*P*) and (ultra)high-temperature ((U)H*T*) granulite terranes record lots of information for understanding lower continental crustal evolution and reconstruction of Precambrain plate tectonics (Rudnick, 1992; O'Brien and Rötzler, 2003; Brown, 2006, 2007; Santosh and Kusky, 2010; Zhai and Liu, 2001; Zhai et al., 1992, 1995, 2001; Zhai, 2009; Zhai and Santosh, 2011). In northern margin of the North China Craton (NCC), both granulite terranes are widely exposed, and considerable efforts have been taken on the mafic H*P* granulites and retrograde eclogites, accordingly various continent-continent collision and micro-blocks amalgamation models were suggested (e.g., Wang et al., 1991; Zhai et al.,1992, 1995; Zhao et al., 2001;

* Corresponding authors.
E-mail addresses: doctoria@sina.com.cn (H.-F. Zhang), mgzhai@mail.iggcas.ac.cn (M.-G. Zhai).

http://dx.doi.org/10.1016/j.precamres.2016.03.001
0301-9268/

Guo et al., 2002). In contrast, the studies of meta-supracrustal rocks (also named as the khondalite series) are relatively limited, and much attention was paid on the low- to medium-*P* granulite facies metamorphism as illustrated by cordierite- and sillimanite-bearing assemblages (e.g., Yan et al.,1991, 1996; Lu et al., 1996).

However, in some localities, the khondalite series are closely associated with mafic H*P* granulites, in this context, one important issue that whether the petrogenesis and geodynamic significance of these granulite terranes are closely related or irrelevant is still ambiguous and hotly debated. In the model of Zhao et al. (2005), the pelitic granulites from the khondalite series in north central part of the NCC were considered to be metamorphosed at medium-pressure (M*P*) granulite facies. They were interpreted to be allochthonous and exotic terranes from the Western Block during the final assembly of the Eastern and Western Blocks at ~1.85 Ga (Zhao et al., 2005, 2010). While, Zhang et al. (1994) interpreted that the khondalite series and mafic H*P* granulites-bearing gray gneisses represented the allochthonous cover and basement, respectively. They were spatially metamorphosed at different crustal levels during one metamorphic event, and juxtaposed by a large low-angle normal shear zone during a late deformation event (Zhang et al., 1994). Liu and Li (2009) proposed that the H*T*–UH*T* khondalite series from south-central Inner Mongolia, and the H*P* granulites from Huai'an-Xuanhua area, northwestern Hebei province together formed high temperature paired metamorphic belts, indicating that both types of granulites underwent entirely different *P*–*T* conditions during a collision event at ~1.92–1.90 Ga. In contrast, Zhai (2009) emphasized that these two types of granulite terranes should have similar metamorphic and deformation history (Zhai et al., 2010; Zhai and Santosh, 2011; Zhang et al., 2014, 2016).

In this contribution, relict kyanite-garnet-K-feldspar assemblages are found in the pelitic granulites from Manjinggou of the Huai'an Complex, suggesting the pelitic granulites suffered comparable H*P* granulite facies metamorphism with associated mafic granulites. Detailed petrological studies and thermodynamic modeling are performed to reconstruct metamorphic evolution of the pelitic granulites. Finally, the metamorphic history, petrogenetic links and their geological implications of the pelitic and mafic H*P* granulites from the Huai'an Complex are discussed.

2. Geological setting

Paleoproterozoic tectonic evolution of the NCC is characterized by three mobile belts (orogenic belts): the Fengzhen mobile belt (Khondalite belt or Inner Mongolia Suture Zone), Jinyu mobile belt (Trans-North China Orogen), and Liaoji mobile belt (Jiao-Liao-Ji belt) (Fig. 1a; Zhai and Liu, 2003; Zhai and Santosh, 2011; Zhao and Zhai, 2013; Santosh, 2010; Zhao et al., 2005). They documented a series of rift-subduction-accretion-collision processes beginning at ~2.35–2.30 Ga and ending at ~2.0–1.97 Ga, illustrating as ~2.3–2.0 Ga magmatic activities with continental rift- or arc-like geochemistry affinity, followed by intensive deformation and low-grade metamorphism (e.g., Zhai and Liu, 2003; Zhai and Peng, 2007; Wang et al., 2010a; Du et al., 2012). During late Paleoproterozoic, the basement of the NCC witnessed two episodes of intensive and extensive metamorphism: ~1.95–1.92 Ga H*P*–(U)H*T* granulite facies metamorphism and ~1.85–1.80 Ga granulite to amphibolite facies retrogression, which may correspond to the assembly or break-up of the Columbia supercontinent (e.g., Zhai and Santosh, 2011; Santosh, 2010; Santosh et al., 2006, 2009, 2013; Kusky et al., 2007).

The Huai'an Complex is located at north central part of the NCC, where is the first locality for discovery of early Precambrain mafic H*P* granulite terranes in the NCC. It is adjacent to east of the Fengzhen mobile belt and north of the Jinyu mobile belt, or at the conjunction of the Khondalite belt and TNCO. It consists mainly of dome-like high-grade metamorphic basements, which are dominated by Archean gray gneisses with minor meta-supracrustal rocks, Paleoproterozoic mafic H*P* granulites, khondalite series and granitic gneisses (Fig. 1a, b). It provides a unique window not only for the study of early Precambrain continental crustal evolution of the NCC, but also for the petrogenesis and geodynamic setting of the Paleoproterozoic extreme crustal H*P*-(U)H*T* granulite facies metamorphism (e.g., Qian et al., 1985; Shen et al., 1992; Zhao et al., 1993, 2008, 2010; Bai et al., 1996; Zhai et al.,1992, 2003; Guo et al., 1993, 2002, 2005; Dirks et al., 1997; Lu et al., 1996; Yan et al., 1996; Wu and Zhong, 1998; Liu, 1995, 1997; Liu et al., 1996, 2002a, 2002b, 2012; Zhang et al., 1994, 2006a, 2006b, 2009, 2011, 2012, 2014, 2016; Wang et al., 2010b, 2011a, 2011b, 2015; Peng et al., 2014; Qu et al., 2012). The Manjinggou outcrop is about 50 km away to southeast of Huai'an county, and consists of six lithological units: the Shuigoukou gray gneisses, banded gneisses, mafic H*P* granulites, khondalite series, Dongjiagou granitic gneiss and Dapinggou garnet-bearing granite from north to south (Fig. 2a; Guo et al., 1993, 2002; Zhao et al., 2008, 2010).

The Shuigoukou gray gneisses are part of the Huai'an TTG gneisses, consist mainly of dioritic, tonalitic, trondjmetic and granodioritic gneisses, and have suffered multi-stages intensive deformation and high-grade metamorphism (e.g., Zhang et al., 1994; Dirks et al., 1997; Zhao et al., 2008). Minor charno-enderbite plutons (~1.85 Ga, Zhao et al., 2008) occur as patches within the gray gneisses. The banded gneisses are composed of interlayered mafic and tonalitic gneisses, and include numerous mafic H*P* granulites lens. Published geochronological data indicate that the emplacement ages of the Shuigoukou gray gneisses and banded gneisses are earlier than ~2.44–2.50 Ga (Zhao et al., 2008; Zhang et al., 2011, 2012).

The mafic H*P* granulites mainly occur as lens or dismembered dykes within the banded gneisses, suggesting the protoliths of mafic H*P* granulite terranes are gabbroic dykes or sills, with minor as xenoliths in the Dongjiagou granitic gneiss and Dapinggou granite (e.g., Fig. 2a; Guo et al., 2002; Zhang et al., 2006a). Zhai et al. (1992) and Guo et al. (2002) performed detailed petrological studies for the mafic H*P* granulites and recognized four generations mineral assemblages ranging from pre-peak (M_1), peak (M_2), post-peak decompression (M_3) to later cooling processes (M_4). The metamorphic peak conditions were retrieved at 11–15 kbar, 750–870 °C using traditional geothermo-barometries. Two layers of khondalite series are exposed in the Manjinggou outcrop, adjacent to the mafic H*P* granulites-bearing banded gneisses or gray gneisses, and consist mainly of garnet-bearing quartzo-feldspathic gneiss, garnet-sillimanite bearing gneiss, with minor calc-sillicates and marbles (Figs. 2a, b; 3a–c). Locally, anatectic leucosomes alternate with the pelitic granulites, or occur as irregularly small granitic pods. Few detailed petrological studies have been focused on the khondalite series, which were considered to be metamorphosed at M*P* granulite facies (e.g., Liu, 1995; Guo et al., 2002; Zhao et al., 2005, 2008, 2010). Available geochronological data revealed that both types of granulite terranes had similar metamorphic ages of ~1.95–1.80 Ga, although different zircon genesis and tectonic implications were proposed (e.g., Zhao et al., 2008, 2010; Guo et al., 2005; Wang et al., 2010b; Zhai, 2009; Zhang et al., 2006b, 2016).

The Dongjiagou granitic gneiss (~2.04 Ga) and the Dapinggou garnet-bearing granite (~1.85 Ga) are only exposed in the southern part of the study area. More detailed information can be found in Zhao et al. (2008). All of the lithological units are truncated or intruded by late pegmatitic granitic veins, such as ~1.81 Ga hyalophane-rich pegmatite veins, which were interpreted to be generated by partial melting of H*P* granulite terrains during uplift to upper to middle crustal levels (Qu et al., 2012).

Structurally, three episodes deformation (D_1–D_3) are recognized in the Huai'an Complex (e.g., Zhang et al., 1994, 2006a, 2009, 2014;

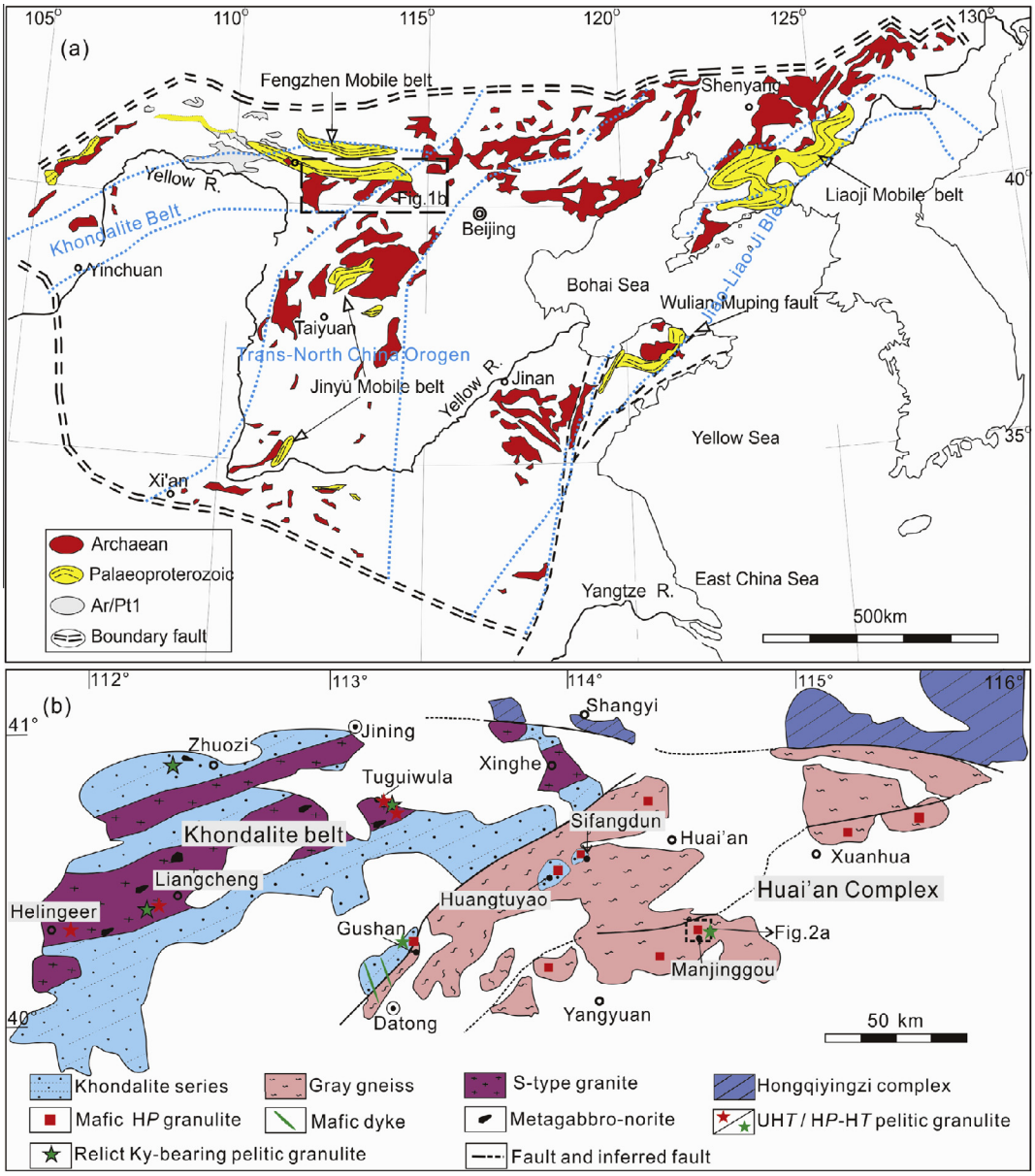

Fig. 1. (a) Paleoproterozoic mobile belts and distribution of early Precambrian rocks in the NCC (Zhai and Liu, 2003). Dashed blue lines represent the boundary of three different continental collisonal orogenic belts proposed by Zhao et al. (2005). (b) Regional geological sketch map of the Huai'an Complex and Khondalite belt in north-central portion of the NCC (modified after Zhai et al., 2003). (For interpretation of the references to colour in this figure legend, the reader is referred to the web version of this article.)

Zhao et al., 2010). The early deformation (D_1) is represented by rootless intrafolial folds preserved locally in some layers of the gray gneisses, mafic HP granulites and khondalite series. It is reworked by pervasive and intensive secondary deformation (D_2), which is characterized by penetrative EW trending foliations (S_2) within all metamorphosed lithological units. Locally, oriented symplectites are around garnet porphyroblasts in the garnet-bearing mafic granulites. It is suggested that the HT–HP peak metamorphism (M_2) predates D_1, while the retrograde MP granulite facies stages (M_3) predates or coincides with D_2. D_3 is characterized by large scale open folds accompanying with retrograde metamorphism (M_3 to M_4) during uplift and cooling stages.

3. Analytical methods

Chemical compositions of minerals were analyzed with a Jeol JXA-8230 electron microprobe. The experiment was performed under conditions of 15 kV accelerating voltage, 10 nA probe current with a 1-μm diameter beam, and the data were regressed using ZAF correction method. The polymorphs of Al_2SiO_5 were verified by Raman spectrograph of Invia model produced by Renishaw Company, with the optical maser wavelength of 514 nm, and scan range from 100 to 1800 cm^{-1}. Major element compositions of the whole rock were analyzed by XRF (Rigku RIX 2100). Above all experiments were conducted at the State Key Laboratory of Continental Dynamics, Northwest University, China.

4. Petrology of pelitic high-pressure granulites

4.1. Petrography

The samples (MJG3, MJG5) were collected 1 km away from the northeast of Manjinggou village (Fig. 2a, b). They are coarse-grained garnet-sillimanite-K-feldspar gneisses, with mineral assemblages of quartz (40–55%), garnet (15–30%), K-feldspar (10–30%), sillimanite (5–15%), biotite (3–10%), kyanite (<1%),

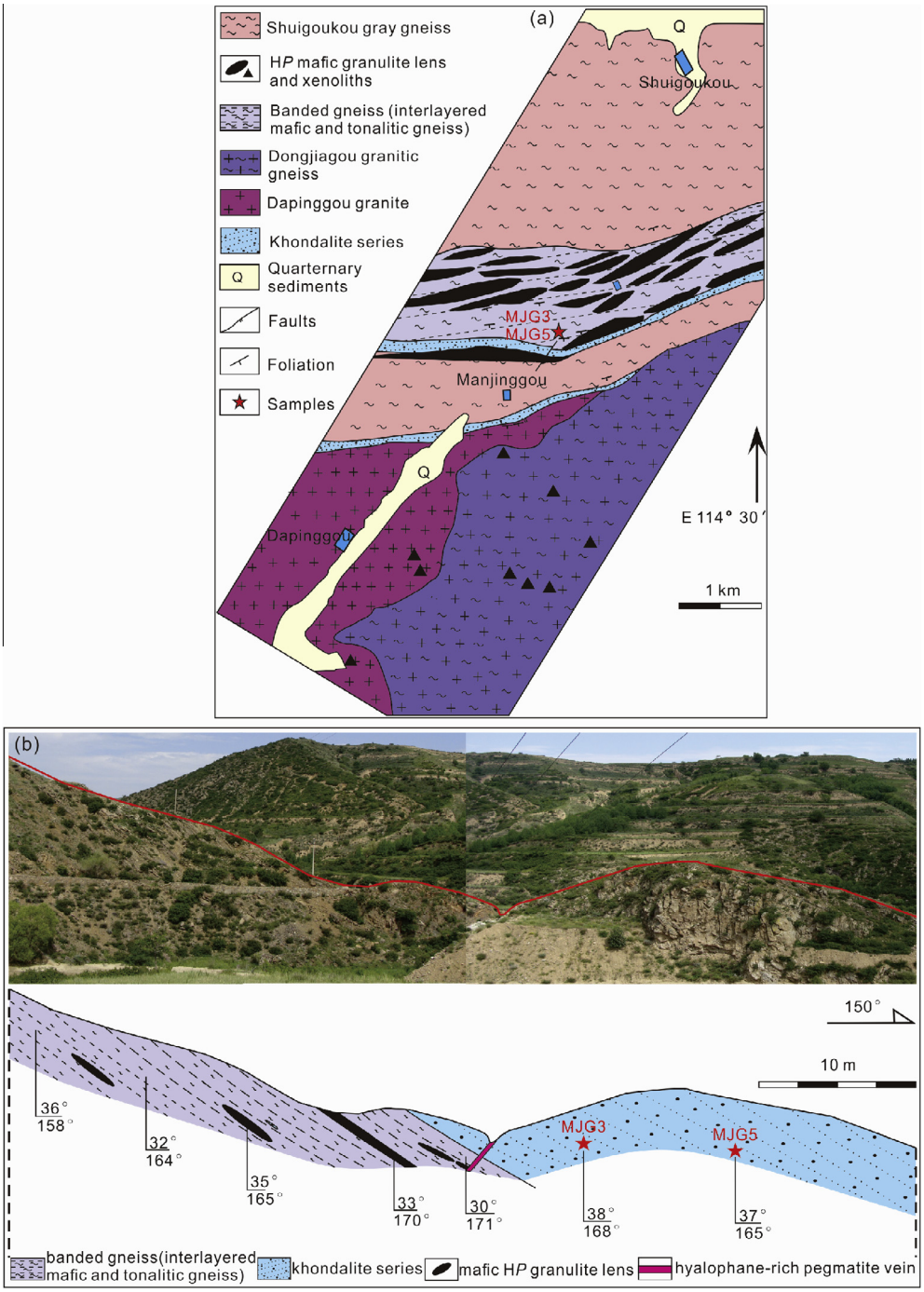

Fig. 2. (a) Geological sketch map showing major lithological units of Manjinggou area of the Huai'an Complex, NCC (after Guo et al., 2002). (b) A representative geological cross section from Manjinggou area.

plagioclase (<5%), muscovite (<3%), with minor rutile, spinel, ilmenite, graphite, pyrite and pyrrhotite (indicative of very low oxygen fugacity) (Fig. 3b, d, r). Kyanites are tested by Raman spectra as shown in the inset of Fig. 3e, i, k. The porphyroblastic garnets, with size of 0.8–2 mm in diameter, show corroded morphology, and are surrounded by perthite, quartz, locally by secondary biotite, muscovite and plagioclase (Fig. 3d, g, k). The mineral inclusions show zoned patterns: (1) a diablastic core crowed with quartz, minor muscovite, biotite and rutile, sometimes rare grains illustrating weak orientation possibly representing an early foliation, (2) an inclusion-rare mantle with discrete kyanite + quartz ± biotite ± muscovite ± rutile ± K-feldspar ± spinel, (3) and an overgrown thin rim developed around some garnet grains with a few inclusions of sillimanite ± biotite ± quartz ± monazite ± rutile ± K-feldspar ± quartz ± spinel (Fig. 3e, f, i, j). Additionally, lots of oriented rutile needles can be observed in the core and mantle of garnets (not shown here), indicating that these rocks possibly suffered relatively high temperature and pressure metamorphic processes (Ague and Eckert, 2012).

Sillimanite can be divided into three groups by occurrence: (1) as acicular inclusions or needles at the rim of porphyroblastic garnets, and sometimes within K-feldspar and quartz, possibly related to breakdown of mica, as reactions (R1) and (R2) illustrated (Fig. 3i, j, p); (2) as idioblastic laths in matrix, and sometimes with

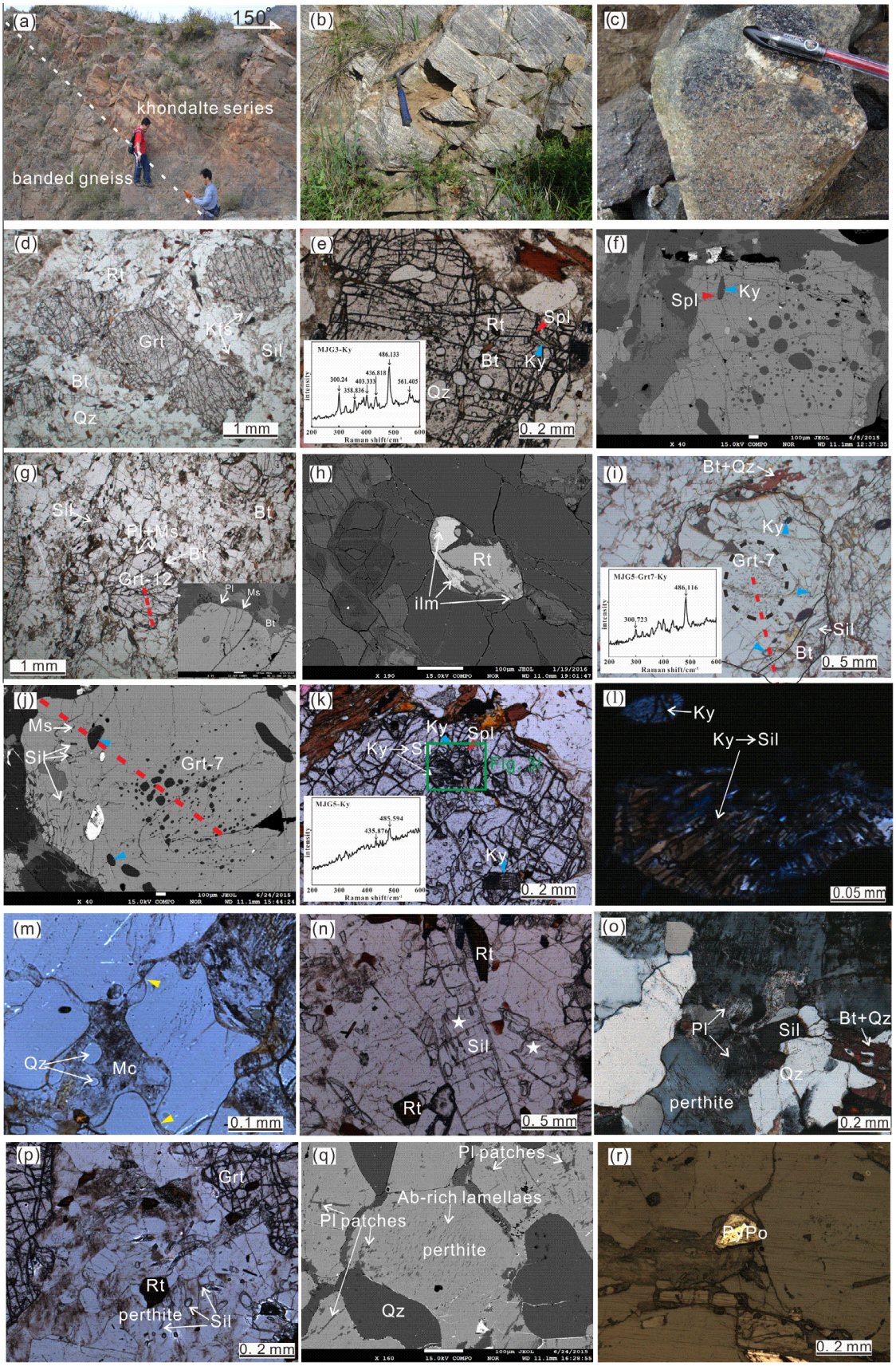
(a)
150°
khondalte series
banded gneiss
(b)
(c)
(d)
Rt
Grt
Ky
Sil
Bt
Qz
1 mm
(e)
Rt
Spl
Bt
Ky
Qz
MJG3-Ky
0. 2 mm
(f)
Spl
Ky
(g)
Sil
Pl
Ms
Bt
Grt-12
1 mm
(h)
Rt
ilm
(i)
Bt+Qz
Ky
Grt-7
MJG5-Grt7-Ky
Sil
Bt
0. 5 mm
(j)
Ms
Sil
Grt-7
(k)
Ky
Spl
Ky→Sil
Qtz
MJG5-Ky
Ky
0. 2 mm
(l)
Ky
Ky→Sil
0.05 mm
(m)
Qz
Mc
0.1 mm
(n)
Rt
Sil
Rt
0. 5 mm
(o)
Pl
Sil
Bt+Qz
Qz
perthite
0.2 mm
(p)
Grt
Rt
perthite
Sil
0. 2 mm
(q)
Pl patches
Ab-rich lamellaes
Pl patches
perthite
Qz
(r)
Py
Po
0. 2 mm

corroded boundaries, which might be as a result of inverse of reaction (R2) (Fig. 3n); (3) as pseudomorphs of kyanite following reaction (R3) (Fig. 3k, l). Kyanite grains are only recognized as inclusions within garnet (Fig. 3e, i, k), with minor as pseudomorphs within garnet or in matrix (Fig. 3k, l).

$$\text{Muscovite} + \text{quartz} \pm \text{plagioclase} = \text{kyanite/sillimanite} + \text{K-feldspar} + \text{melt}. \quad (R1)$$

$$\text{Biotite} + \text{quartz} \pm \text{plagioclase} = \text{garnet} + \text{kyanite/sillimanite} + \text{K-feldspar} + \text{melt}. \quad (R2)$$

$$\text{Kyanite} = \text{sillimanite}. \quad (R3)$$

Plagioclase grains are rarely observed in the investigated samples, a few are around embayed garnets (Fig. 3g), and others are interstitial (Fig. 3o), with minor grains occurring as irregular patches within perthite (Fig. 3q). The less amounts of plagioclase might be controlled by low CaO and Na_2O content in bulk composition, alternatively pertinent to reactions (R1) and (R2) which are at the expense of plagioclase during prograde metamorphism. K-feldspar grains with irregular morphology include two types of variants: perthite and microline (Fig. 3m, p, q). The perthite grains including some small sillimanite grains (Fig. 3p) are possibly as peritectic products of reactions (R1) and (R2), and some microline grains with cuspate and irregular shapes apparently seem to be solidification of melt (Fig. 3m).

Biotite appears mainly in three textural domains, the first type is included in garnet grains (Fig. 3e, i), the second type is discrete flake in matrix (Fig. 3d, g), and the third type is intergrown with quartz around garnet, indicative of melting reaction (R2) operating in reverse during retrograde metamorphic stages (Fig. 3i, k). Locally, a few biotite flakes are intergrown with muscovites. Muscovites are rarely preserved as relict inclusions in garnet core or mantle (Fig. 3j), or as flakes in matrix. The latter with lobate or flake shapes shows replacement of pre-existed garnet, feldspar or sillimanite.

Spinel occurs as inclusion in the mantle and rim of garnet porphyroblast, with or without contact with kyanite, and no direct contact with quartz (Fig.3e, f, k). Zircon and monazite grains are observed as mineral inclusions in garnet, sillimanite and K-feldspar, or as single grain in matrix. Rutile is distributed pervasively in matrix, locally moated by ilmenite (Fig. 3h), indicative of decompression retrogression.

4.2. Mineral chemistry

Sample MJG5 was selected for detailed mineral composition analysis, and representative minerals compositions are given in Appendix A. Tables S1 and S2.

Garnet in the examined sample is dominated by almandine and pyrope, with minor grossular (<7 mol.%) and negligible spessartine (<1 mol.%), without significant composition zoning, except for slightly rim-ward increase of almandine and decrease of grossular and pyrope contents ($Alm_{58-64}Prp_{32-36}Grs_{4-7}Sps_{0-1}$) (Fig. 4 and Appendix A. Table S1). For instance, Grt-7 and Grt-12 exhibit rim-ward decreasing X_{Grs} and increasing X_{Alm}, with $X_{Grs} = \sim 0.06$, $X_{Alm} = 0.58–0.60$ from the core to mantle, and $X_{Grs} = 0.04$, $X_{Alm} = 0.64$ in the rim. The relatively homogenous composition from core to mantle might be due to re-equilibrium during metamorphic peak stages, while the decreasing X_{Grs} in the rim is consistent with decompression-driven growth of garnet (e.g., Pattison and Begin, 1994; Spear et al., 1990; Cooke et al., 2000).

Biotites exhibit high TiO_2 content (4.20–5.81 wt.%) and variable X_{Mg} (0.63–0.75). The biotites contacting with garnets, either as inclusions or at the rim of garnets, have relatively higher X_{Mg} (0.70–0.75), while those off garnets exhibit lower X_{Mg} (0.63–0.68; Appendix A. Table S2). The higher X_{Mg} might be attributed to partial or complete re-equilibrium with garnet during retrograde evolution (e.g., Spear and Florence, 1992). Muscovite grains included in the mantle of garnet exhibit high content of SiO_2 (49.29–51.92 wt.%), suggesting a relatively high-pressure condition. In contrast, the secondary muscovites in matrix display low content of SiO_2 (47.11 wt.%) (Appendix A. Table S2).

Plagioclases around garnet rim and in matrix exhibit narrow range of X_{An} (0.43–0.46). Some plagioclase grains, displaying irregular patches within perthite (Fig. 3q), exhibit relatively large variation in X_{An} (0.32–0.45), and possibly represent crystals recrystallized from melt or metasomatised by fluids (Appendix A. Table S2). The host crystals of perthites are orthoclase-rich ($X_{Or} = 0.82–0.91$, $X_{An} = 0–0.02$), and the exsolution lamellaes are albite-rich ($X_{Ab} = 0.85–0.94$, $X_{An} = 0.01–0.05$). The host microclines have slightly high orthoclase ($X_{Or} = 0.96$, $X_{An} = 0$), and the exsolution lamellaes are rich in albite component ($X_{Ab} = 0.88$, $X_{An} = 0.03$) (Appendix A. Table S2).

The spinel grains in the investigated samples are gahnitic spinel: those contacted with kyanites displaying higher ZnO content of 15.36–15.49 wt.%, than those off kyanites (8.17–8.87 wt.%) (Appendix A. Table S2).

4.3. Metamorphic mineral assemblages evolution

Based on textural evolution and mineral chemistry of samples, four generations of mineral assemblages are recognized: pre-peak (M_1), peak (M_2), and post-peak assemblages (M_3 and M_4). Pre-peak assemblage (M_1) is characterized by the mineral inclusions within garnet core, namely, garnet core + biotite + rutile + quartz ± muscovite ± plagioclase. Peak assemblage (M_2) is composed of garnet mantle and its inclusions of kyanite + rutile + biotite + K-feldspar + quart ± muscovite ± gahnitic spinel, representing H*P* granulite facies stage. Post-peak decompression assemblage (M_3) consists of garnet rim + sillimanite + quartz + biotite + K-feldspar + rutile + plagioclase ± gahnitic spinel, representing the imprinted M*P* granulite facies stage. The mineral assemblages and reaction textures from granulite to amphibolite facies (M_4) retrogression are not obvious, with minor intergrowth of biotite and quartz around embayed garnet, and

Fig. 3. Representative field photographs and photomicrographs of pelitic granulites in Manjingou area of the Huai'an Complex, NCC. (a) The boundary between the mafic H*P* granulite-bearing banded gneisses and khondalite series. (b) The pelitic H*P* granulite. (c) The mafic H*P* granulite. (d) Sample MJG3, garnets with corroded boundaries. Mineral abbreviations after Whitney and Evans (2010): Bt-biotite, Grt-garnet, Kfs-K-feldspar, Mc-microline, Ms-muscovite, Ky-kyanite, Pl-plagioclase, Py-pyrite, Po-phyrrhotite, Qz-quartz, Rt-rutile, Sil-sillimanite, Spl-spinel. (e) Close up of garnet from MJG3, with Qz, Bt, Rt, Ky and Spl inclusions. Red and blue triangulars denote gahnitic spinels and kyanites, respectively. Raman spectra of kyanite is also shown in the inset. (f) BSE image of garnet from (e). (g) Sample MJG5, plagioclase, biotite and muscovite around Grt-12 (see the BSE image in the inset). Red dashed line represents selected composition profiles. (h) Rutile is moated by ilmenite. (i, j) Grt-7 from MJG5 with inclusion-zoned pattern, see detail in the text. (k) Kyanite and the transition from kyanite to sillimanite are preserved in garnet. (l) Close up of (k). (m) Recrystallized string-of-beads texture developed between quartz and microline as pointed by yellow triangular. Some rounded quartz grains are included within microline. (n) Sillimanite with embayed boundary at the site of white stars. (o) Intergrowth of biotite and quartz grains around garnet (garnet is not shown here), with a few plagioclase grains in matrix. (p) Sillimanite grains included in perthite. (q) BSE image of perthite with albite-rich exsolution lamellaes. Note that some irregular plagioclase patches within perthites. (r) Reflected light micrograph showing the texture of pyrite and phyrrhotite. (For interpretation of the references to colour in this figure legend, the reader is referred to the web version of this article.)

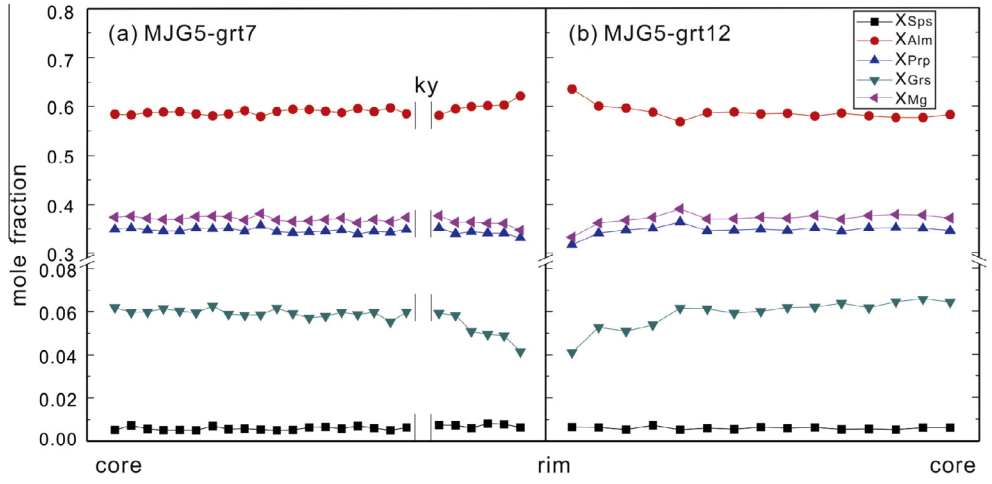

Fig. 4. Compositional profiles of the porphyroblastic garnet (Grt-7 and Grt-12) of sample MJG5. The selected profiles are shown in Fig. 3g, i, j.

Table 1
Composition of measured bulk composition, added melt and melt re-integrated protolith of sample MJG5 (in mol.%).

Measured bulk composition									
H_2O	SiO_2	Al_2O_3	CaO	MgO	FeO	K_2O	Na_2O	TiO_2	O
1.46	72.49	11.52	0.82	3.92	6.34	2.16	0.73	0.59	0.01
Added melt composition									
P (kbar)	T (°C)	H_2O	SiO_2	Al_2O_3	CaO	MgO	FeO	K_2O	Na_2O
14	809.8	28.40	56.12	7.61	0.79	0.14	0.38	2.53	4.03
Melt re-integrated protolith									
H_2O	SiO_2	Al_2O_3	CaO	MgO	FeO	K_2O	Na_2O	TiO_2	O
4.97	70.33	11.01	0.82	3.43	5.56	2.21	1.16	0.51	0.01

replacement of rutile by ilmenite, or growth of secondary muscovite.

5. Phase equilibrium modeling

P–T pseudosections were calculated in the Na_2O-CaO-K_2O-FeO-MgO-Al_2O_3-SiO_2-H_2O-TiO_2-O (NCKFMASHTO) system, which is currently the most realistic components system to approximate natural rocks (e.g., White et al., 2007). MnO was not included due to its low content in the investigated sample, and no significant influence on the phase relationships at high *P–T* conditions (e.g., White et al., 2007). ZnO was not included, due to the lack of Zn-bearing silicate thermodynamic components in the database of Holland and Powell (1998, 2011), therefore, the phase relationships of spinel in the pseudosections are inconsistent with those in the investigated samples. The oxides composition measured by XRF were choosen as the bulk composition, except for O and H_2O (see Table 1). The proportion of O was assumed at a minimum value of O = 0.01 mol.%, as sulfide and graphite are observed in our samples (e.g., Indares et al., 2008). The content of water was estimated by volume of biotite using the Ti–H substitution assumption of White et al. (2007). Thermocalc v.3.33 (Powell and Holland, 1988 and updates) and the internally-consistent dataset of Holland and Powell (1998) were used. The phases involved in the thermodynamic modeling and corresponding a-x relationships are: garnet, liquid (silicate melt) and biotite (White et al., 2007), plagioclase and K-feldspar (Holland and Powell, 2003), muscovite (Coggon and Holland, 2002), cordierite (Holland and Powell, 1998), ilmenite (White et al., 2000) and spinel (White et al., 2002), kyanite, sillimanite, rutile and quartz.

The preservation of peak assemblages and migmatitic textures of the pelitic granulites from Manjingou area indicate that an early partial melting and melt loss event possibly occurred during pre-peak to peak metamorphic stages (e.g., White and Powell, 2002). Therefore, the oxide bulk composition measured by XRF represents refractory composition after melt loss instead of fertile protolith before melt extract from the system (e.g., White et al., 2004; Indares et al., 2008). It was used to approximate near-peak to peak and retrograde evolution. A melt re-integration technique was used to recover the protolith before melt loss, and then to assess the possible prograde evolution (e.g., White et al., 2004; Indares et al., 2008; Groppo et al., 2012).

5.1. *P–T* pseudosections calculated with measured bulk composition

P–T pseudosections were conducted in the *P–T* range of 5–15 kbar, 700–920 °C (Fig. 5; Appendix B. Fig. S1). In this *P–T* range, garnet, K-feldspar and quartz are always present. In higher pressure, melt firstly arises at the expense of muscovite, quartz and plagioclase, followed by disappearance of plagioclase, muscovite, and then biotite up to 850–860 °C. Among 7–8 kbar, ilmenite becomes stable at the expense of rutile. Corderite and spinel arise with the consumption of biotite, sillimanite, quartz and garnet in the *HT–LP* region (see mineral modes evolution in the Appendix B. Fig. S1a,b,c). The isopleths of mineral modes are near parallel to pressure coordinate in the biotite-liquid bearing assemblages, indicating that they are sensitive to temperature change. The contours of X_{Grs} of garnet are flatter, increasing with pressure in a wide *P–T* space, and are useful indicator of pressure. The isopleths of X_{Prp} of garnet and X_{Mg} of biotite are sub-parallel to the pressure axis within supra-solidus field, except for the biotite-absent assemblages. It is suggested that both of them are useful indicators of temperature: the higher the value of X_{Prp} (Grt) and X_{Mg}(Bt), the higher temperature (Appendix B. Fig. S1d,e).

As shown in Fig. 5b, the preserved *HP* granulite facies mineral assemblages (Grt-Ky-Kfs-Bt-Rt-Qz-Liq±Ms) are restricted to

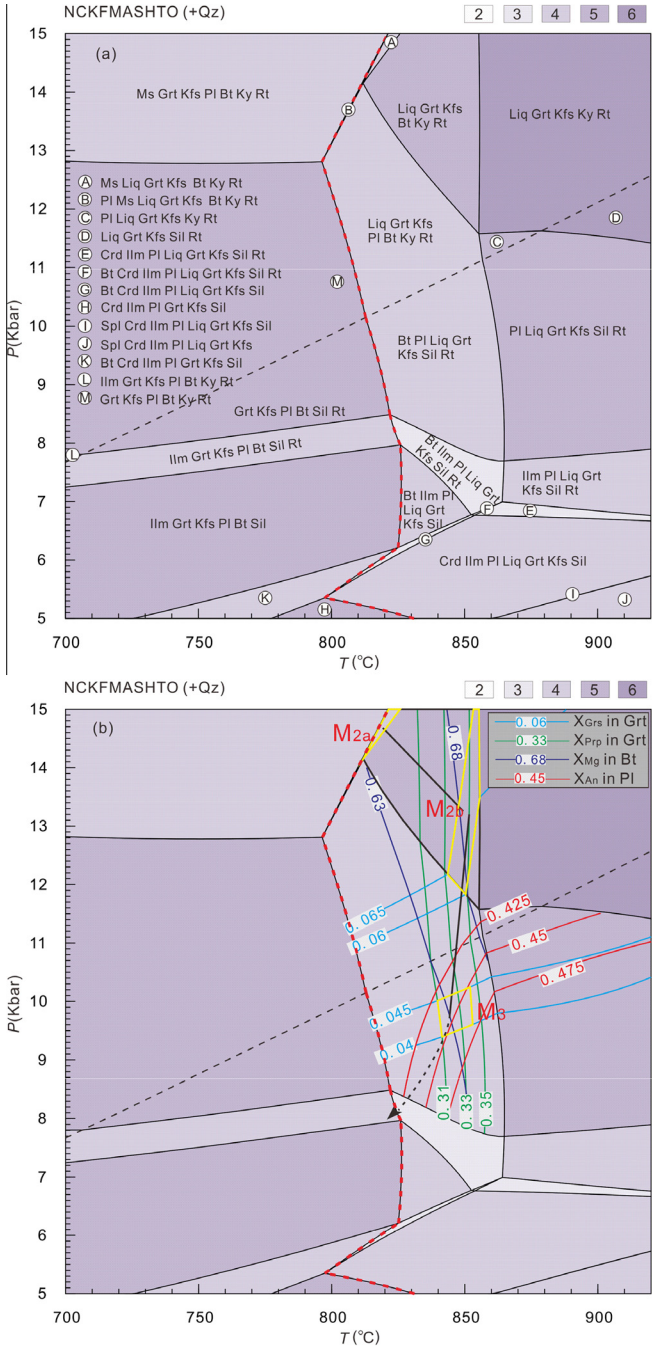

Fig. 5. (a) *P–T* pseudosections calculated from measured bulk composition of sample MJG5. (b) The stability field of metamorphic peak assemblages Grt-Kfs-Ky-Bt-Rt-Liq-Qz±Ms is confined by black bold lines in the *P–T* space. M_{2a} represents the stability field of Grt-Kfs-Ky-Bt-Rt-Liq-Qz-Ms, M_{2b} represents the isopleths intersection of X_{Grs} and X_{Prp} of garnet mantle or X_{Mg}(Bt), and M_3 represents the isopleths intersection of X_{Grs} and X_{Prp} of garnet rim or X_{Mg}(Bt), X_{An}, see detail in text. Mineral abbreviations after Whitney and Evans (2010).

>11.5 kbar, 810–860 °C in the *P–T* space, similar to published results of pelitic H*P* granulites from Helanshan, northwestern margin of the NCC (e.g., Zhou et al., 2010). The muscovite-bearing assemblage (Grt-Ky-Kfs-Bt-Rt-Qz-Liq-Ms; named as M_{2a}), as shown in the mantle of Grt-7 (Fig. 3i, j), is confined in a *P–T* range of >14 kbar, >810 °C. The intersection of composition isopleths of garnet mantle (the site of kyanite inclusions: X_{Grs} = 0.060–0.065, X_{Prp} = 0.35) is plotted in the field of muscovite-free assemblage (Grt-Ky-Kfs-Bt-Rt-Qz-Liq; named as M_{2b}), within *P–T* range of 12.2–14.5 kbar, ~855 °C. It is similar to the results by using the identical X_{Grs} and highest X_{Mg} of biotite in matrix off garnet (X_{Grs} = 0.06–0.065, X_{Mg}(Bt) = 0.68): 12–13.5 kbar, ~850 °C. Therefore, the reasonable *P–T* conditions of H*P* granulite facies are 11.5–15 kbar, 810–860 °C.

The *P–T* conditions of M*P* granulite facies (Grt-Sil-Kfs-Pl-Bt-Rt-Liq-Qz, M_3) are constrained at ~9.5 kbar, ~850 °C, using the composition of garnet rim (X_{Grs} = 0.04, X_{Prp} = 0.32), or combination with the minimum X_{Mg}(Bt) = 0.63, or X_{An} = 0.43–0.46 in matrix (Fig. 5b). A further decompression-cooling evolution might be constrained by replacement of rutile by ilmenite at ~6.5–8.5 kbar, and ceased when the melt solidified (~820 °C, Fig. 5b; Indares et al., 2008). It is consistent with appearance of corderite in other samples in the same region (e.g., Zhao et al., 2010). However, the appearance of muscovite in matrix is difficult to account for using such a set of pseudosections, which might be pertinent to local hydration reactions within sub-solidus field, and a further discussion is listed at Section 6.1. Therefore, a *P–T* segment from peak (M_{2a} to M_{2b}) to retrograde (M_3 to solidus) evolution of sample MJG5 can be constrained as Fig. 5b.

5.2. *P–T* pseudosections calculated with melt re-integrated bulk composition

The melt re-integration technique was from Indares et al. (2008) and Groppo et al. (2012), and one step of melt loss was assumed. The composition of the added melt was calculated at 14 kbar, 809.8 °C, which represent the *P–T* conditions of melt loss occurred at the intersection of a hypothetical prograde *P–T* path and solidus of measured bulk composition. 15 mol.% melt was added so that this rock immediately below the solidus is just H_2O-saturated at a moderate to high pressure (10.11 kbar, 670.6 °C, outside of the *P–T* space presented here; e.g., White et al., 2001, 2004; Indares et al., 2008; Groppo et al., 2012). The compositions of added melt and melt re-integrated protolith are listed in Table 1.

Pseudosections calculated with melt re-integrated bulk composition are illustrated as Fig. 6 and Appendix B. Fig. S2, and the solidus of measured bulk composition is also shown as red dashed line for reference (e.g., Indares et al., 2008). The topologies to the right of the reference line are similar to that calculated from refractory measured bulk composition within supra-solidus fields, except for some difference in the H*T*–L*P* conditions. For example, K-feldspar becomes instable in fertile melt re-integrated composition, but always stable in refractory composition. In contrast, the topologies to left of the reference line are dramatically different. The liquid-bearing and muscovite-bearing assemblages become stable in a wide *P–T* space, garnet becomes instable at L*T*–L*P* areas, and K-feldspar is absent in the L*T*–H*P* muscovite-bearing fields. The distribution patterns of mineral composition and mode isopleths are similar to those calculated from refractory composition, and the difference lies mainly in the expanding muscovite-bearing fields and the increasing mode of liquid at the equivalent *P–T* conditions (Appendix B. Fig. S2a,b,c). The mode of liquid increases with temperature, with a sharp increase from appearance of K-feldspar to muscovite-out boundary, and increases continuously in the muscovite-absent fields, which is related to the progress of reactions R1 and R2. The mode isopleths of garnet show a flatter pattern, and increase continuously in the muscovite-bearing fields (sensitive to pressure). In contrast, in the muscovite-absent fields, they exhibit a near vertical pattern (sensitive to temperature). The isopleths of X_{An} in plagioclase and X_{Grs} in garnet are complementary in many assemblages (Appendix B. Fig. S2d,e).

As mentioned above, such a set of pseudosections are useful to constrain the possible prograde evolution. For our samples, the prograde evolution is difficult to reconstruct using relict mineral

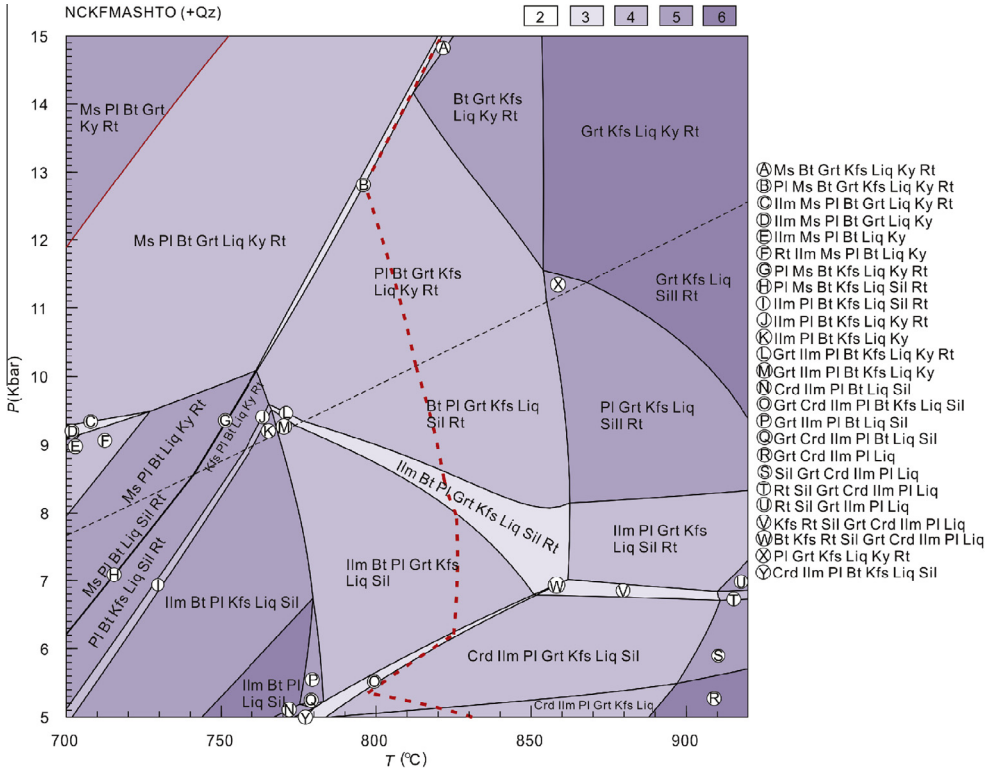

Fig. 6. *P–T* pseudosections calculated from melt re-integrated bulk composition of sample MJG5. The red solid line represents solidus of melt re-integrated composition, and the red dashed line presented here represents solidus calculated from measured bulk composition for reference, mineral abbreviations from Fig. 5. (For interpretation of the references to color in this figure legend, the reader is referred to the web version of this article.)

composition due to long dwelling time at HT conditions, but some relict mineral inclusions within robust and indissolvable garnets can possibly provide important information for pre-peak or peak metamorphic evolution. The patterns of the inclusions (quartz, rutile, biotite, muscovite, kyanite and sillimanite) within the porphyroblastic garnets show regular zonation (see Section 4.3; Fig. 3i), suggesting that the growth of zoned garnet is probably within various mineral stability fields. In this context, the texture development of inclusion patterns of zoned garnet is a useful *P–T* indicator. The detailed prograde *P–T* evolution is assessed at Section 5.3.

5.3. Prograde evolution based on inclusion patterns of zoned garnet

A set of composite pseudosections (Fig. 7) based on combination with individual pseudosection calculated from melt re-integrated and melt refractory compositions are constructed to assess the *P–T* evolution of the investigated samples (e.g., Indares et al., 2008). The left part of reference line (solidus of measured bulk composition) is extracted from pseudosection using melt re-integrated composition (Fig. 6), which is useful to assess the prograde evolution. The right part is extracted from that calculated from measured bulk composition (Fig. 5), which is used to approximate the peak and retrograde evolution of the samples (see Section 5.1).

Textural evolution of metamorphic rocks documents lots of clues to metamorphic evolution of investigated samples, which can be linked to the mineral modes development (e.g., Stüwe and Powell, 1995). In this context, the modes (volume proportions) of zoned garnet were used to constrain the metamorphic evolution. Supposed that the growth of garnet was continuous and accumulative, without consumption during prograde and peak stage evolution, and a spherical model for garnet of MJG5 was used. The volume proportions of zoned garnet are estimated: inclusion-crowed core (~5–10%), inclusion-rare mantle (~70–90%, kyanite ± muscovite bearing domains), and the overgrown rim (0–10%, sillimanite-bearing domians), respectively. They correspond to the modes of garnet during prograde (~1–2 mol.%), near peak to peak (~14–18 mol.%) and retrograde (~0–2 mol.%) stages, assuming that the total mode of garnet was 20 mol.% in MJG5. In the Appendix C, we took Grt-7 from sample MJG5 as an example for detailed calculation processes of the proportions of zoned garnet. The muscovite grains are preserved in outer mantle of garnet, suggesting that the growth of garnet core and mantle possibly within the stability field of muscovite. In the muscovite-bearing fields, the proportion of garnet increases with pressure. Therefore, a possible prograde *P–T* vector from M_1 to M_{2a} is constrained as black dashed line (Fig. 7b). Note that the slope of prograde vector is apparently subparallel to the composition isopleths (X_{Grs} = 0.06–0.07, Fig. 7b) of garnet. It is suggested that X_{Grs} of the garnet (core and mantle) in sample MJG5 from prograde to near-peak or peak stages is likely without substantial change. The corroded garnet grains indicate that garnets are consumed during decompression, consistent with the appearance of intergrown biotite and quartz, plagioclase and muscovite around garnet, although sillimanite-bearing thin layers are overgrown at the rim of some garnet grains. Therefore, the estimated ~14–18 mol.% garnet at near peak conditions is minimum, which is consistent with *P–T* vector from M_{2a} (~19–21 mol.%) to M_{2b} (~21–25 mol.%) inferred in Figs. 7b and 5b.

6. Disucssion

6.1. Metamorphic P–T evolution of the HT–HP granulites from Manjinggou area

The *P–T* results of the pelitic granulites in this study are different from those of previous studies that the pelitic granulites were assumed as metamorphosed at MP granulite facies conditions

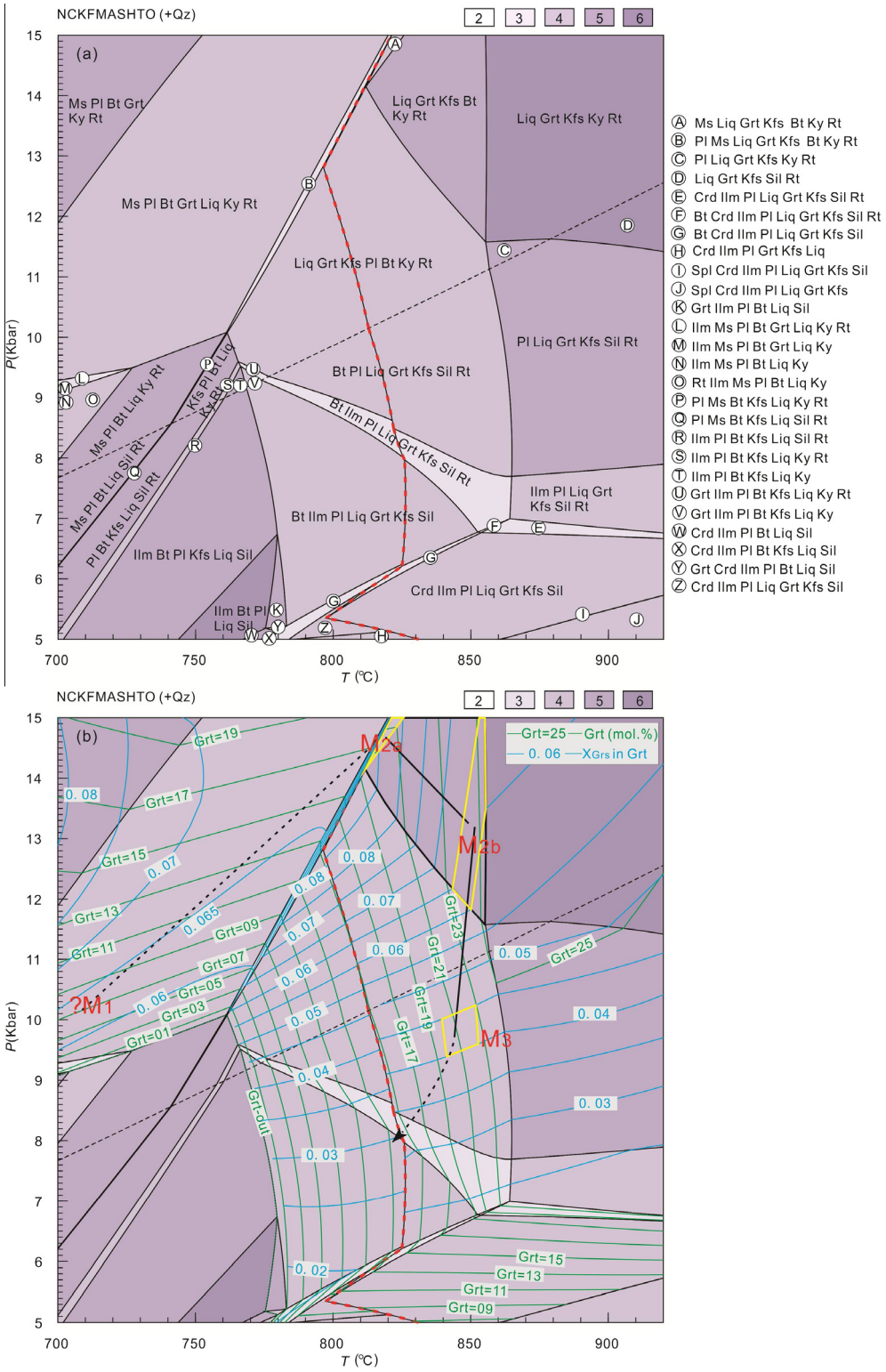

Fig. 7. (a) Composite *P–T* pseudosections combination with those calculated from measured and melt re-integrated bulk composition of sample MJG5. The left part of red dashed line (solidus of measured bulk composition) is extracted from pseudosections using melt re-integrated composition, while the right part is extracted from that calculated from measured bulk composition. (b) *P–T* path inferred from textural and mineral composition development, see detail in text. The red dashed line and mineral abbreviations after Fig. 5. (For interpretation of the references to color in this figure legend, the reader is referred to the web version of this article.)

(8–10 kbar, 750–850 °C; Lu and Jin, 1993; Liu, 1997). It can be attributed to be free of recognized Ky-Grt-Kfs assemblages, or re-equilibrium of mineral composition. For example, the pelitic granulites from Manjinggou area were previously considered to be metamorphosed at the sillimanite stability field (Liu, 1995; Guo et al., 2002; Zhao et al., 2005, 2008, 2010). Lu and Jin (1993) reported kyanite-bearing assemblages in pelitic granulites from the Ji'ning Complex. However, they interpreted them as prograde assemblages based on combined GB and GASP geothermobarometries with the composition of garnet and included biotite, plagioclase and kyanite. It is known that the Fe-Mg exchange between garnet and included biotite is easily re-equilibrated during

retrograde stage for high grade metamorphic rocks. Consequently, the calculated temperatures are lower than peak stages, and result in lower pressures (e.g., Lu and Jin, 1993; Liu, 1997).

In this paper, composition isopleths of single garnet are used to estimate the *P–T* conditions, and the X_{Grs}, X_{Prp} are useful *P*, *T* indicators, respectively (Appendix B. Fig. S1d). The results are consistent with stability field of preserved mineral assemblages (Grt-Ky-Kfs-Bt-Rt-Qz-Liq±Ms), within the *P–T* range of 11.5–15 kbar, 810–860 °C. It is then imprinted by intensive M*P* granulite facies (~9.5 kbar, ~850 °C), and characterized by transition from kyanite to sillimanite with decreasing X_{Grs} in garnet, similar to previously assumed metamorphic peak conditions (e.g., Lu and Jin, 1993; Liu, 1997). As to spinels, those contacted with kyanites exhibiting relatively high content of ZnO (15.36–15.49 wt.%), might be formed at H*P* granulite facies stage; in contrast, those off kyanites in the rim of garnet with relatively low ZnO (8.17–8.87 wt.%) might be formed within sillimanite stability field at M*P* granulite facies. These are highly consistent with the experimental results in the FeO-MgO-Al_2O_3-SiO_2-ZnO system, in which the additional ZnO would enlarge and expand the stability field of spinel toward relatively higher pressures and lower temperatures (Nichols et al., 1992). During decompression and cooling stages, the retrograde assemblages of pelitic granulites are often preserved at the intersection of retrograde *P–T* path and solidus (Grt-Sil-Kfs-Pl-Bt-Qz-Ru-Ilm (Liq = 0); Fig. 5b), where melt are crystallized (e.g., White et al., 2002; Indares et al., 2008; Groppo et al., 2012). The mineral assemblages and reaction textures of the studied pelitic granulites are not well developed during sub-solidus cooling stage from granulite facies to amphibolite facies (M_4). A retrograde temperature (~650 °C, If P = 5–7 kbar) was estimated from re-equilibrium between contacted biotite and garnet using the GB thermometer of Holdaway (2000). As a result, the decompression (I*T*D segment) and cooling (IBC segment) *P–T* paths from peak to retrograde stages were reconstructed (see Fig. 8).

In addition, the inclusion patterns of zoned garnets in the pelitic granulite suggest a pressure and temperature increasing process (from M_1 to M_{2a}, Fig. 7b) before arriving at metamorphic peak stage. However, the metamorphic age of increasing pressure stage and more metamorphic evidences are insufficient to establish a complete *P–T*-t path for the pelitic granulites, especially the prograde metamorphic *P–T* paths. Therefore, further study is still needed for detailed petrogenetic processes or burying history of the pelitic granulites.

This case study gives us an excellent example to recognize H*P* granulites in the extensively re-equilibrated high-grade metasupracrustal rocks, which inspires us to conduct more detailed work on the mineral inclusions of robust minerals, such as garnet and zircon for the khondalite series from the NCC. For mafic H*P* granulites, the metamorphic textural development and *P–T* evolution are comparable. The metamorphic peak assemblages are dominated by Grt-Cpx-Pl-Qz-Rt, with relatively high X_{Grs} and X_{Prp} in garnet, slightly high Na_2O and Al_2O_3 contents in clinopyroxene and low X_{An} in plagioclase (e.g., Cooke et al., 2000), with recoverable peak conditions of 11–14.5 kbar, 750–870 °C (Guo et al., 2002; Zhai et al., 1992). The imprinted M*P* granulite facies metamorphism (8.5–10.5 kbar, 770–830 °C), is characterized by corona of orthopyroxene and plagioclase, and some clinopyroxene grains with fingerprint-like plagioclases, defining a near-isothermal decompression (I*T*D) *P–T* segment (Fig. 8). The fine grains symplectite of amphibole and plagioclase developed well around garnets, which defines a near-isobaric cooling (IBC) *P–T* segment from medium- to low-pressure granulite to amphibolite facies (Fig. 8; Zhai et al., 1992; Guo et al., 2002).

6.2. Implications for metamorphic history of granulite from the Huai'an Complex

It is still an open issue whether the pelitic and mafic granulites were metamorphosed during one metamorphic episode with similar metamorphic *P–T* conditions (e.g., Zhang et al., 1994, 2014, 2016; Zhao et al., 2010; Zhai, 2009). Previously, field and structural geological work demonstrate that both types of granulite terranes are closely interlayered with the same foliations, indicating their

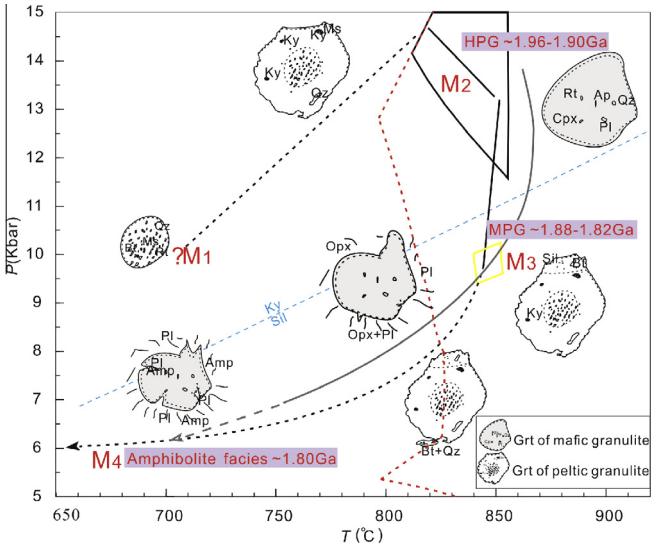

Fig. 8. Metamorphic *P–T* evolution of H*T*–H*P* granulites from Manjinggou area. The prograde and supra-solidus *P–T* segment of pelitic granulites is from Fig. 7b, and an extension *P–T* segment during the cooling stage from granulite to amphibolite facies was estimated from re-equilibrium between contacted garnet and biotite. *P–T* path of the mafic granulites (gray line) is after Zhai et al. (1992). Red dashed line represents solidus of measured bulk composition. The four generations of mineral assemblages of the pelitic granulites are as follow. M_1: Grt core and Qz-Bt-Rt±Ms±Pl inclusions; M_2: Grt mantle and Ky-Bt-Qz-Rt-Kfs±Ms inclusions; M_3: Grt rim and Kfs-Sil-Bt-Qz-Pl-Rt in matrix; and the retrograde cooling stages from granulite to amphobolite facies with intergrowth of Bt and Qz around Grt, replacement of Rt by Ilm, and appearance of secondary muscovites (not shown here). The mafic H*P* granulites developed with characterized peak assemblages (M_2): Grt-Cpx-Pl-Qz-Rt; retrograde M*P* to L*P* granulite facies assemblages (M_3): Opx-Cpx-Pl-Qz±Grt; retrograde amphibolite facies assemblages (M_4): Amp-Pl±Grt. (For interpretation of the references to colour in this figure legend, the reader is referred to the web version of this article.)

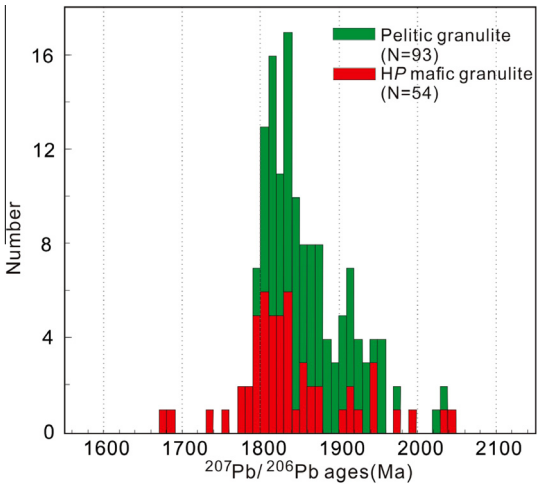

Fig. 9. Compilation of metamorphic ages of both types of granulite terranes from Manjinggou area, and the data were selected from published SHRIMP zircons geochronological data of Zhao et al. (2010) and Guo et al. (2005).

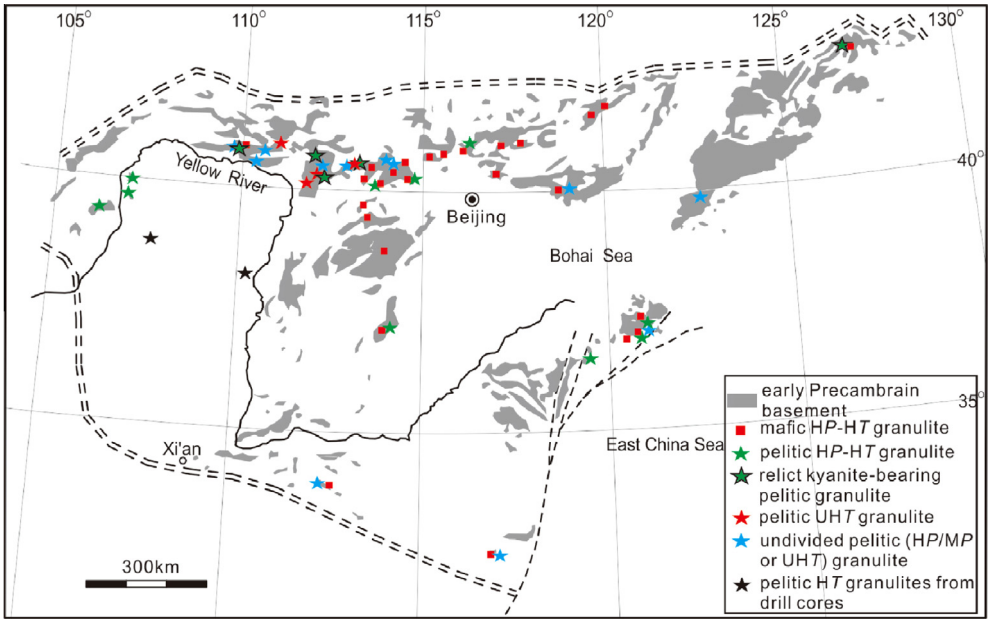

Fig. 10. Spitial distribution of HT–HP or HT–UHT granulites in the NCC.

similar metamorphic and deformation history (e.g. Zhang et al., 2014; Zhai, 2009). Herein, the direct petrological evidence supports the consideration that the khondalite series and garnet-bearing mafic granulites suffered similar metamorphic *P–T* conditions. Consistently, published metamorphic ages of both types of granulite terranes in the studied area also exhibit two comparable peaks (Fig. 9; ~1.96–1.90 Ga and ~1.88–1.82 Ga; Zhao et al., 2010; Guo et al., 2005), respectively corresponding to HP and MP granulite facies stages (e.g., Zhang et al., 2006b, 2016; Zhai, 2009). Therefore, both types of granulites from Manjinggou area were experienced the same metamorphic history from peak stage during ~1.96–1.90 Ga to retrograde stages (~1.88–1.80 Ga; Fig. 8). It is different from the views that pelitic rocks and associated mafic granulites are different slabs with individual metamorphic history (e.g. Zhang et al., 1994; Zhao et al., 2005, 2008, 2010).

The fact that pelitic and associated mafic granulites from Manjinggou underwent the same metamorphic history is not an isolate case. Field work also document that in other localities, such as Daqingshan and Huangtuyao of Inner Mongolia, Gushan and Sifangdun of Shanxi province, the protolith of the mafic HP granulites intruded the khondalite series as dykes, and then deformed and metamorphosed together (e.g., Zhang et al., 2014; Zhai, 2009; Liu et al., 2015; Fig. 1b), although the estimated pressures of the khondalite series are lower than those of the associated mafic granulites. It is noteworthy that we have also recognized kyanite-bearing pelitic HP granulites in Gushan, Datong, about 150 km away to the southeast of Manjinggou area (unpublished data). Additionally, in some localities, such as Daqingshan area, Zhuozi, Liangcheng and Qianqi of Inner Mongolia, where UHT metamorphic rocks were documented, relict kyanites were also reported (Figs. 1b; 10; Liu et al., 1993, 2002a,b; Lu and Jin, 1993; Cui, 1987; Wang et al., 2011b). The rarely relict kyanites in garnet porphyroblasts and extensive sillimanite in matrix of the pelitic granulites are likely attributed to long dwell time (~1.88–1.82 Ga) under medium- to low-*P* granulites facies conditions. Consequently, the khondalite series exposed in the easternmost portion of the Khondalite Belt and Huai'an Complex, were probably experienced HP granulite facies metamorphism, but previously derived MP granulite facies conditions might be attributed to mineral re-equilibrium in retrogression. Much more detailed work are still needed.

6.3. Implications for Paleoproterozoic tectonic mechanisms

Fig. 10 illustrates the distribution of Paleoproterozoic granulites in the NCC. It seems to indicate that the granulite facies rocks are widely exposed in the basement, except for some locations covered by Phanerozoic sediments. Published metamorphic peak conditions of those granulites are in the *P–T* range of 7–15 kbar, 750–900 °C, except for those UHT granulites of 6.5–9 kbar (up to >11 kbar), >900 °C (Zhai, 2009, and reference therein). The apparent geothermal gradients can be estimated at ~16–25 °C/km for HP granulites, ~25–40 °C/km for UHT granulites, within the regime of low- to medium-P/T facies series of Miyashiro (1973), different from HP–UHP rocks (~6 °C/km for Dabie UHP rocks) under modern plate tectonic regime. The estimated exhumation rates of theses granulite terranes from HP (assumed at ~45–50 km, ~1.95 Ga) to MP (assumed at ~30 km, ~1.85 Ga) granulite facies stages, then via low-*P* granulite facies to amphibolite facies (assumed at ~15–25 km, ~1.80 Ga) and to earth surface at ~1.78 Ga are ~0.15–0.2 mm/yr, ~0.1–0.3 mm/yr and ~0.75–1.25 mm/yr, respectively. They are several to tens times slower than HP–UHP rocks formed in the Phanerozoic continental collisional belts. Therefore, the widespread distribution, higher apparent geothermal gradients and slower exhumation rate, as well as long dwell time at high temperature conditions of these HT–HP granulite terranes from the NCC seems to indicate that the thermal regimes and tectonic mechanisms of Paleoproterozoic probably differ from those of Phanerozoic eons, and these granulite terranes were likely formed in a hot and slow cooling orogen (e.g., Ashwal et al., 1999; Högdahl et al., 2012).

7. Conclusions

1. The relict Grt-Ky-Kfs bearing assemblages of the pelitic granulites are stabilized around 11.5–15 kbar, 810–860 °C, and the imprinted MP granulite facies are stabilized at ~9.5 kbar, ~850 °C, defining a characterized near isothermal

decompression *P–T* path. The inclusion patterns of zoned garnets indicate that a *P–T* increasing process before metamorphic peak stage, however, no sufficient metamorphic evidences to reconstruct the *P–T*-t path so far, as well as the tectonic mechanisms to bring the pelitic rocks down to lower crustal level.

2. The newly recognized pelitic H*P* granulites from Manjinggou area provide direct petrological evidence that these two types of granulites shared the same metamorphic history from peak to retrograde stages, consistent with field geological observations and published geochronological data. This fact changes our previous thinking, i.e. pelitic rocks and associated mafic granulites are different slabs with individual metamorphic history.
3. The khondalite series exposed in the easternmost portion of the Khondalite Belt and Huai'an Complex, were experienced H*P* granulite facies metamorphism, but previously derived M*P* granulite facies conditions might be attributed to mineral re-equilibrium in retrogression.
4. The widespread distribution, higher apparent geothermal gradient and slower exhumation rate of these Paleoproterozoic H*T*–H*P* granulite terranes in the NCC differ from H*P*–UH*P* rocks formed in the Phanerozoic continental collisional belts. It may indicate that the thermal regimes and tectonic mechanisms of Paleoproterozoic probably differ from those of Phanerozoic eons. These granulite terranes were likely formed in a hot and slow cooling orogen.

Acknowledgements

The Chief editor Prof. Guochun Zhao and two anonymous reviewers are thanked for their constructive comments. The first author is indebted to Dr. Tiesheng Li for his help in discussions about the contents and language expressions. Dr. Ligang Zhou and doctoral students Zhichao Li, Yongsheng Gai, Xiaoying Liao are appreciated for their helpful discussion. This study was financially supported by the 973 program (Grant No. 2012CB4166006) funded by the State Ministry of Science and Technology, and research programs (Grant Nos. 41530208) supported by the National Natural Science Foundation of China.

Appendix A. Supplementary data

Supplementary data associated with this article can be found, in the online version, at http://dx.doi.org/10.1016/j.precamres.2016.03.001.

References

Ague, J.J., Eckert, J.O., 2012. Precipitation of rutile and ilmenite needles in garnet: implications for extreme metamorphic conditions in the Acadian Orogen, USA. Am. Mineral. 97, 840–855.
Ashwal, L.D., Tucker, R.D., Zinner, E.K., 1999. Slow cooling of deep crustal granulites and Pb-loss in zircon. Geochim. Cosmochim. Acta 63, 2839–2851.
Bai, J., Huang, X.G., Dai, F.Y., Wu, C.H., 1996. The Precambrian Evolution of China, second ed. Geological Publishing House, Beijing, pp. 24–32 (in Chinese).
Brown, M., 2006. Duality of thermal regimes is the distinctive characteristic of plate tectonics since the Neoarchean. Geology 34, 961–964.
Brown, M., 2007. Metamorphic conditions in orogenic belts: a record of secular change. Int. Geol. Rev. 49, 193–234.
Coggon, R., Holland, T.J.B., 2002. Mixing properties of phengitic micas and revised garnet-phengite thermobarometers. J. Metamorph. Geol. 20, 683–696.
Cooke, R.A., O'Brien, P.J., Carswell, D.A., 2000. Garnet zoning and the identification of equilibrium mineral compositions in high-pressure-temperature granulites from the Moldanubian zone, Austria. J. Metamorph. Geol. 18, 551–569.
Cui, W.Y., 1987. Mineralogy and metamorphic *P–T* conditions of granulite-facies rocks from Jining-Huai'an district. J. Changchun College of Geol., Special Issue, 165–189 (in Chinese).
Dirks, P.H.G.M., Zhang, J.S., Passchier, C.W., 1997. Exhumation of high-pressure granulites and the role of lower crustal advection in the north china craton near Datong. J. Struct. Geol. 19, 1343–1358.
Du, L.L., Yang, C.H., Ren, L.D., Song, H.X., Geng, Y.S., Wan, Y.S., 2012. The 2.2-2.1 Ga magmatic event and its tectonic implication in the Lüliang Mountains, North China Craton. Acta Petrolog. Sin. 28, 2751–2769 (in Chinese with English abstract).
Groppo, C., Rolfo, F., Indares, A., 2012. Partial melting in the Higher Himalayan Crystallines of Eastern Nepal: the effect of decompression and implications for the 'Channel flow' model. J. Petrol. 53, 1057–1088.
Guo, J.H., Zhai, M.G., Zhang, Y.G., Li, Y.G., Yan, Y.H., Zhang, W.H., 1993. Huai'an-Manjinggou early Precambrian high-pressure granulite mélanges: geological characteristics, petrology and isotopic chronology. Acta Petrolog. Sin. 9, 1–13 (in Chinese with English abstract).
Guo, J.H., O'Brien, P.J., Zhai, M.G., 2002. High-pressure granulites in the Sanggan area, North China Craton: metamorphic evolution, *P–T* paths and geotectonic significance. J. Metamorph. Geol. 20, 741–756.
Guo, J.H., Sun, M., Chen, F.K., Zhai, M.G., 2005. Sm-Nd and SHRIMP U-Pb zircon geochronology of high-pressure granulites in the Sanggan area, North China Craton: timing of Paleoproterozoic continental collision. J. Asian Earth Sci. 24, 629–642.
Högdahl, K., Majka, J., Sjöström, H., Nilsson, K.P., Claesson, S., Konečný, P., 2012. Reactive monazite and robust zircon growth in diatexites and leucogranites from a hot, slowly cooled orogen: implications for the Palaeoproterozoic tectonic evolution of the central Fennoscandian Shield, Sweden. Contrib. Miner. Petrol. 163, 167–188.
Holdaway, M.J., 2000. Application of new experimental and garnet Margules data to the garnet-biotite geothermometer. Am. Mineral. 85, 881–892.
Holland, T.J.B., Powell, R., 1998. An internally consistent thermodynamic data set for phases of petrological interest. J. Metamorph. Geol. 16, 309–343.
Holland, T.J.B., Powell, R., 2003. Activity-composition relations for phases in petrological calculations: an asymmetric multicomponent formulation. Contrib. Miner. Petrol. 145, 492–501.
Holland, T.J.B., Powell, R., 2011. An improved and extended internally consistent thermodynamic dataset for phases of petrological interest, involving a new equation of state for solids. J. Metamorph. Geol. 29, 333–383.
Indares, A., White, R.W., Powell, R., 2008. Phase equilibria modelling of kyanite-bearing anatectic paragneisses from the central Grenville Province. J. Metamorph. Geol. 26, 815–836.
Kusky, T.M., Li, J.H., Santosh, M., 2007. The Paleoproterozoic North Hebei Orogen: North China Craton's collisional suture with Columbia supercontinent. Gondwana Res. 12, 4–28.
Liu, F.L., 1995. Metamorphic mineral-fluid evolution and tectonic environments of the granulite facies terrane in the Huaian-Datong area (in Chinese) Ph. D. thesis. Changchun University of Earth Sciences, Changchun, p. 136.
Liu, F.L., 1997. The mineral evolution and geodynamic significance of excess-Alumino gneiss on the bordering area of Jin-Inner Mongolia. J Geol Miner. Res. North China 12, 337–346 (in Chinese with English abstract).
Liu, S.J., Li, J.H., 2009. Paleoproterozoic high temperature paired metamorphic belt in central part of Southern Inner Mongolia and its tectonic implication. Geol. J. China Univ. 15, 48–56.
Liu, X.S., Jin, W., Li, S.X., Xu, X.C., 1993. Two types of Precambrain high-grade metamorphism, Inner Mongolia, China. J. Metamorph. Geol. 11, 499–510.
Liu, S.W., Shen, Q.H., Geng, Y.S., 1996. Metamorphic evolution of two types of garnet-granulites in northwestern Heibei province and analyses by Gibbs method. Acta Petrolog. Sin. 12, 261–275 (in Chinese with English abstract).
Liu, F.L., Shen, Q.H., Zhao, Z.R., Geng, Y.S., Katayama, I., 2002a. Identification of high-pressure mineral assemblages in garnet mafic granulites, Northwestern Hebei province: evidence from mineral inclusions in Zircons. Acta Geol. Sinica 76, 209–217.
Liu, F.L., Shen, Q.H., Zhao, Z.R., 2002b. Evolution of mineral assemblages of khondalite series in the process of prograde metamorphism, southern Inner Mongolia. Geol. Bull. China 21, 75–78 (in Chinese with English abstract).
Liu, F., Guo, J.H., Peng, P., Qian, Q., 2012. Zircon U-Pb ages and geochemistry of the Huai'an TTG gneisses terrane: petrogenesis and implications for 2.5 Ga crustal growth in the North China Craton. Precambr. Res. 213, 225–244.
Liu, P.H., Liu, F.L., Cai, J., Wang, F., Liu, J.H., Liu, C.H., Wang, W., Liu, L.S., Shi, J.R., 2015. Discovery and geological implications of high-P mafic granulites from Daqingshan-Wulashan, the Khondalite belt of North China Craton. In: Abstract Volume of 2015 Annual meeting of Chinese Geoscience Union, Beijing, pp. 339–340 (in Chinese).
Lu, L.Z., Jin, S.Q., 1993. P-T-t paths and tectonic history of an early Precambrain granulite facies terrane, Jining district, south-east Inner Mongolia, China. J. Metamorph. Geol. 11, 483–498.
Lu, L.Z., Xu, X.C., Liu, F.L., 1996. The Precambrian Khondalite Series in Northern China. Changchun Publishing House, Changchun, pp. 59–67.
Miyashiro, A., 1973. Metamorphism and Metamorphic belts. George Allen and Unwin, London, p. 492.
Nichols, G.T., Berry, R.F., Green, D.H., 1992. Internally consistent gahnitic spinel-cordierite-garnet equilibria in the FMASHZn system: geothermobarometry and applications. Contrib. Miner. Petrol. 111, 362–377.
O'Brien, P.J., Rötzler, J., 2003. High-pressure granulites: formation, recovery of peak conditions and implications for tectonics. J. Metamorph. Geol. 21, 3–20.
Pattison, R.M., Begin, N.J., 1994. Zoning patterns in orthopyroxene and garnet in granulite: implications for geothermometry. J. Metamorph. Geol. 12, 387–410.
Peng, P., Wang, X.P., Windley, B.F., Guo, J.H., Zhai, M.G., Li, Y., 2014. Spatial distribution of ~1950-1800 Ma metamorphic events in the North China Craton: implications for tectonic subdivision of the craton. Lithos 202, 250–266.
Powell, R., Holland, T.J.B., 1988. An internally consistent dataset with uncertainties and correlations 3: applications to geobarometry, worked examples and a computer program. J. Metamorph. Geol. 6, 173–204.

Qian, X.L., Cui, W.Y., Wang, S.Q., 1985. Evolution of the Nei Mongol-Eastern Hebei Archaean granulite Belt in the North china Craton. The records of Geological Research. Peking University Press, Beijing, pp. 20–29 (in Chinese with English abstract).

Qu, M., Guo, J.H., Lai, Y., Peng, P., Liu, F., 2012. Origin and geological significance of the 1.81 Ga hyalophane-rich pegmatite veins from the high-pressure granulite terrain in the Central Zone of North China Craton. Sci. China Earth Sci. 55, 193–203. http://dx.doi.org/10.1007/s11430-011-4330-y.

Rudnick, R.L., 1992. Xenoliths-Samples of the lower continental crust. In: Fountain, D.M., Arculus, R., Kay, R.W. (Eds.), Continental Lower Crust. Elsevier, Amsterdam, pp. 269–316.

Santosh, M., 2010. Assembling North China Craton within the Columbia supercontinent: the role of double-sided subduction. Precambr. Res. 178, 149–167.

Santosh, M., Kusky, T., 2010. Origin of paired high pressure-ultrahigh-temperature orogens: a ridge subduction and slab window model. Terra Nova 22, 35–42.

Santosh, M., Sajeev, K., Li, J.H., 2006. Extreme crustal metamorphism during Columbia supercontinent assembly: evidence from the North China Craton. Gondwana Res. 10, 256–266.

Santosh, M., Wan, Y.S., Liu, D.Y., Dong, C.Y., Li, J.H., 2009. Anatomy of zircons from an ultrahot orogen: the amalgamation of the North China Craton within the supercontinent Columbia. J. Geol. 117, 429–443.

Santosh, M., Liu, D., Shi, Y., Liu, S.J., 2013. Paleoproterozoic accretionary orogenesis in the North China Craton: a SHRIMP zircon study. Precambr. Res. 227, 29–54.

Shen, Q.H., Xu, H.F., Zhang, Z.Q., Gao, J.E., Wu, J.S., Ji, C.L., 1992. Granulites of Early Precambrian in China. Geological Publishing House, Beijing, pp. 221–223 (in Chinese).

Spear, F.S., Florence, F.P., 1992. Thermobarometry in granulites: pitfalls and new approaches. Precambrain Res. 55, 209–241.

Spear, F.S., Kohn, M.J., Florence, F.P., Menard, T., 1990. A model for garnet and plagioclase growth in pelitic schists: implications for thermobarometry and P–T path determinations. J. Metamorph. Geol. 8, 683–696.

Stüwe, K., Powell, R., 1995. PT paths from modal proportions: application to the Koralm Complex, Eastern Alps. Contrib. Miner. Petrol. 119, 83–93.

Wang, R.M., Chen, Z.Z., Chen, F., 1991. Grey tonalitic gneiss and high-pressure granulite inclusions in Hengshan, Shanxi Province, and their geological significance. Acta Petrolog. Sin. 4, 36–45 (in Chinese with English abstract).

Wang, Z.H., Wilde, S.A., Wan, J.L., 2010a. Tectonic setting and significance of 2.3-2.1 Ga magmatic events in the Trans-North China Orogen: new constraints from the Yanmenguan mafic-ultramafic intrusion in the Hengshan-Wutai-Fuping area. Precambr. Res. 178, 27–42.

Wang, J., Wu, Y.B., Gao, S., Peng, M., Liu, X.C., Zhao, L.S., Zhou, L., Hu, Z.C., Gong, H.J., Liu, Y.S., 2010b. Zircon U-Pb and trace element data from rocks of the Huai'an Complex: new insights into the late Paleoproterozoic collision between the Eastern and Western Blocks of the North China Craton. Precambr. Res. 178, 59–71.

Wang, L.J., Guo, J.H., Peng, P., Liu, F., 2011a. Metamorphic and geochronological study of garnet-bearing basic granulites from Gushan, the eastern end of the Khondalite Belt in the North China Craton. Acta Petrolog. Sin. 27, 3689–3700 (in Chinese with English abstract).

Wang, F., Li, X.P., Chu, H., Zhao, G.C., 2011b. Petrology and metamorphism of khondalites from the Jining complex, North China Craton. Int. Geol. Rev. 53, 212–229.

Wang, L.J., Guo, J.H., Peng, P., Liu, F., Windley, B.F., 2015. Lithological units at the boundary zone between the jining and huai'an complexes (central-northern margin of the north china craton): a Paleoproterozoic tectonic mélange? Lithos 227, 205–224.

White, R.W., Powell, R., 2002. Melt loss and the preservation of granulite facies mineral assemblages. J. Metamorph. Geol. 20, 621–632.

White, R.W., Powell, R., Holland, T.J.B., Worley, B.A., 2000. The effect of TiO_2 and Fe_2O_3 on metapelitic assemblages at greenschist and amphibolite facies conditions: mineral equilibria calculations in the system K_2O-FeO-MgO-Al_2O_3-SiO_2-TiO_2-Fe_2O_3. J. Metamorph. Geol. 18, 497–511.

White, R.W., Powell, R., Holland, T.J.B., 2001. Calculation of partial melting equilibria in the system Na_2O-CaO-K_2O-FeO-MgO-Al_2O_3-SiO_2-H2O (NCKFMASH). J. Metamorph. Geol. 19, 139–153.

White, R.W., Powell, R., Clarke, G.L., 2002. The interpretation of reaction textures in Fe-rich metapelitic granulites of the Musgrave Block, central Australia: constraints from mineral equilibria calculations in the system K_2O-FeO-MgO-Al_2O_3-SiO_2-TiO_2-Fe_2O_3. J. Metamorph. Geol. 20, 41–55.

White, R.W., Powell, R., Halpin, J.A., 2004. Spatially-focused melt formation in aluminous metapelites from Broken Hill, Australia. J. Metamorph. Geol. 22, 825–845.

White, R.W., Powell, R., Holland, T.J.B., 2007. Progress relating to calculation of partial melting equilibria for metapelites. J. Metamorph. Geol. 25, 511–527.

Whitney, D.L., Evans, B.W., 2010. Abbreviations for names of rock-forming minerals. Am. Mineral. 95, 185–187.

Wu, C.H., Zhong, C.T., 1998. The Paleoproterozoic SW-NE collision model for the central North China Craton. Prog. Precambrian Res. 21, 28–50 (in Chinese).

Yan, Y.H., Zhai, M.G., Guo, J.H., 1991. The corderite-sillimanite assemblages in the Archean granulite belt on North China Platform as an indicator for low-pressure granulitie facies. Acta Petrolog. Sin. 4, 47–56 (in Chinese with English abstract).

Yan, Y.H., Li, Y.G., Liu, W.J., 1996. Huai'an massif and Hengshan massif. In: Zhai, M.G. et al. (Eds.), Granulites and Lower Crust in North China Craton. Seismological Press, Beijing, pp. 80–93.

Zhai, M.G., 2009. Two kinds of granulites (HT–HP and HT–UHT) in North China Craton:their genetic relation and geotectonic implications. Acta Petrolog. Sin. 25, 1753–1771 (in Chinese with English abstract).

Zhai, M.G., Liu, W.J., 2001. The formation of granulite and its contribution to evolution of the continental crust. Acta Petrolog. Sin. 17, 28–38 (in Chinese with English abstract).

Zhai, M.G., Liu, W.J., 2003. Palaeoproterozoic tectonic history of the North China Craton: a review. Precambr. Res. 122, 183–199.

Zhai, M.G., Peng, P., 2007. Paleoproterozoic events in North China Craton. Acta Petrolog. Sin. 23, 2665–2682 (in Chinese with English abstract).

Zhai, M.G., Santosh, M., 2011. Early Precambrian odyssey of the North China Craton: a synoptic overview. Gondwana Res. 20, 6–25.

Zhai, M.G., Guo, J.H., Yan, Y.H., Li, Y.G., Zhang, W.H., 1992. Discovery and preliminary study of Archaean high-pressure basic granulites in North China. Sci. China (B) 36, 1402–1408.

Zhai, M.G., Guo, J.H., Li, J.H., Yan, Y.H., Li, Y.G., Zhang, W.H., 1995. The discoveries of retrograde eclogites in North China craton in Archaean. Chin. Sci. Bull. 40, 1590–1594.

Zhai, M.G., Liu, W.J., Guo, J.H., 2001. An oblique cross-section of Precambrian crust in the North China Craton. Phys. Chem. Earth Part A 26, 781–792.

Zhai, M.G., Guo, J.H., Li, Y.G., Liu, W.J., Peng, P., Shi, X., 2003. Two linear granite belts in the central-western north china craton and their implication for late Neoarchaean-Palaeoproterozoic continental evolution. Precambr. Res. 127, 267–283.

Zhai, M.G., Li, T.S., Peng, P., Hu, B., Liu, F., Zhang, Y.B., Guo, J.H., 2010. Precambrian key tectonic events and evolution of the North China Craton. In: Kusky, T.M., Zhai, M.G., Xiao, W.J. (Eds.), The Evolving Continents, vol. 338. Geological Society of London Special Publications, pp. 235–262.

Zhang, J.S., Dirks, P.H.G.M., Passchier, C.W., 1994. Extensional collapse and uplift of a poly-metamorphic granulite terrain in the Archean of north China. Precambr. Res. 67, 37–57.

Zhang, J., Zhao, G.C., Sun, M., Wilde, S.A., Li, S.Z., Liu, S.W., 2006a. High-pressure mafic granulites in the Trans-North China Orogen: tectonic significance and age. Gondwana Res. 9, 349–362.

Zhang, H.F., Zhai, M.G., Peng, P., 2006b. Zircon SHRIMP U-Pb age of the Paleoproterozoic high-pressure granulites from the Sanggan area, North China Craton and its geologic implications. Earth Sci. Front. 13, 190–199 (in Chinese with English abstract).

Zhang, H.F., Luo, Z.B., Zhou, Z.G., Liu, C.F., 2009. Palaeoproterozoic collisional time in the Sanggan area of the North China Craton: constraints from age of regional ductile shearing and post-collisional strongly peraluminous granites. J. Mineral. Petrol. 1, 60–67 (in Chinese with English abstract).

Zhang, H.F., Zhai, M.G., Santosh, M., Diwu, C.R., Li, S.R., 2011. Geochronology and petrogenesis of Neoarchean potassic meta-granites from Huai'an Complex: implications for the evolution of the North China Craton. Gondwana Res. 20, 82–105.

Zhang, H.F., Zhai, M.G., Santosh, M., Diwu, C.R., Li, S.R., 2012. Low-Al and high-Al trondhjemites in the Huai'an Complex, North China Craton: geochemistry, zircon U-Pb and Hf isotopes, and implications for Neoarchean crustal growth and re-melting. J. Asian Earth Sci. 49, 203–213.

Zhang, H.F., Zhai, M.G., Santosh, M., Wang, H.Z., Zhao, L., Ni, Z.Y., 2014. Paleoproterozoic granulites from the Xinghe graphite mine, North China Craton: geology, zircon U-Pb geochronology and implications for the timing of deformation, mineralization and metamorphism. Ore Geol. Rev. 63, 478–497.

Zhang, H.F., Wang, H.Z., Santosh, M., Zhai, M.G., 2016. Zircon U-Pb ages of Paleoproterozoic mafic granulites from the Huai'an terrane, North China Craton (NCC): implications for timing of cratonization. Precambr. Res. 272, 244–263.

Zhao, G.C., Zhai, M.G., 2013. Lithotectonic elements of Precambrian basement in the North China Craton: review and tectonic implications. Gondwana Res. 23, 1207–1240.

Zhao, Z.P. et al., 1993. Precambrian crustal evolution of the Sino-Korean Paraplatform. Science Press, Beijing, pp. 284–330 (in Chinese).

Zhao, G.C., Cawood, P.A., Wilde, S.A., Lu, L.Z., 2001. High-pressure granulites (retrograded eclogites) from the Hengshan Complex, North China Craton: petrology and tectonic implications. J. Petrol. 42, 1142–1170.

Zhao, G.C., Sun, M., Wilde, S.A., Li, S.Z., 2005. Late Archean to Paleoproterozoic evolution of the North China Craton: key issues revisited. Precambr. Res. 136, 177–202.

Zhao, G.C., Wilde, S.A., Sun, M., Guo, J.H., Kröner, A., Li, S.Z., Li, X.P., Wu, C.M., 2008. SHRIMP U-Pb zircon geochronology of the Huai'an Complex: constraints on Late Archean to Paleoproterozoic crustal accretion and collision of the Trans-North China Orogen. Am. J. Sci. 308, 270–303.

Zhao, G.C., Wilde, S.A., Guo, J.H., Cawood, P.A., Sun, M., Li, X.P., 2010. Single zircon grains record two continental collisional events in the North China craton. Precambr. Res. 177, 266–276.

Zhou, X.W., Zhao, G.C., Geng, Y.S., 2010. Helanshan high-pressure pelitic granulites: petrological evidence for collision event in the Western Block of the North China Craton. Acta Petrolog. Sin. 26, 2113–2121.